Graphene metamaterials based tunable terahertz absorber: effective surface conductivity approach

Andryieuski, Andrei; Lavrinenko, Andrei

Published in:
Optics Express

Link to article, DOI:
10.1364/OE.21.009144

Publication date:
2013

Document Version
Publisher's PDF, also known as Version of record

Graphene metamaterials based tunable terahertz absorber: effective surface conductivity approach

Andrei Andryieuski,* and Andrei V. Lavrinenko

DTU Fotonik, Technical University of Denmark, Oersteds pl. 343, Kongens Lyngby, DK-2800, Denmark

**andra@fotonik.dtu.dk*

Abstract: In this paper we present the efficient design of functional thin-film metamaterial devices with the effective surface conductivity approach. As an example, we demonstrate a graphene based perfect absorber. After formulating the requirements to the perfect absorber in terms of surface conductivity we investigate the properties of graphene wire medium and graphene fishnet metamaterials and demonstrate both narrowband and broadband tunable absorbers.

OCIS codes: (310.3915) Metallic, opaque, and absorbing coatings; (050.6624) Subwavelength structures; (160.3918) Metamaterials.

References and links

1. J. Federici and L. Moeller, "Review of terahertz and subterahertz wireless communications," J. Appl. Phys. **107**, 111101 (2010).
2. P. Jepsen, D. Cooke, and M. Koch, "Terahertz spectroscopy and imaging - modern techniques and applications," Laser & Photonics Rev. **5**, 124–166 (2011).
3. M. Tonouchi, "Cutting-edge terahertz technology," Nature (London) **1**, 97–105 (2007).
4. K. Bolotin, K. Sikes, Z. Jiang, M. Klima, G. Fudenberg, J. Hone, P. Kim, and H. Stormer, "Ultrahigh electron mobility in suspended graphene," Solid State Commun. **146**, 351–355 (2008).
5. A. Geim, "Graphene: status and prospects." Science **324**, 1530–1534 (2009).
6. K. S. Novoselov, V. I. Fal'ko, L. Colombo, P. R. Gellert, M. G. Schwab, and K. Kim, "A roadmap for graphene." Nature (London) **490**, 192–200 (2012).
7. J. Chen, M. Badioli, P. Alonso-González, S. Thongrattanasiri, F. Huth, J. Osmond, M. Spasenović, A. Centeno, A. Pesquera, P. Godignon, A. Z. Elorza, N. Camara, F. J. García de Abajo, R. Hillenbrand, and F. H. L. Koppens, "Optical nano-imaging of gate-tunable graphene plasmons." Nature (London) **487**, 77–81 (2012).
8. Z. Fei, A. S. Rodin, G. O. Andreev, W. Bao, A. S. McLeod, M. Wagner, L. M. Zhang, Z. Zhao, M. Thiemens, G. Dominguez, M. M. Fogler, A. H. Castro Neto, C. N. Lau, F. Keilmann, and D. N. Basov, "Gate-tuning of graphene plasmons revealed by infrared nano-imaging." Nature (London) **487**, 82–85 (2012).
9. A. N. Grigorenko, M. Polini, and K. S. Novoselov, "Graphene plasmonics," Nature Photonics **487**, 749–758 (2012).
10. A. Hill, S. A. Mikhailov, and K. Ziegler, "Dielectric function and plasmons in graphene," Europhysics Lett. **87**, 27005 (2009).
11. M. Jablan, H. Buljan, and M. Soljačić, "Plasmonics in graphene at infrared frequencies," Phys. Rev. B **80**, 245435 (2009).
12. F. H. L. Koppens, D. E. Chang, and F. J. G. De Abajo, "Graphene plasmonics: a platform for strong light-matter interactions," Nano Lett. **11**, 3370–3377 (2011).
13. S. Mikhailov and K. Ziegler, "New electromagnetic mode in graphene," Phys. Rev. Lett. **99**, 016803 (2007).
14. A. Vakil and N. Engheta, "Transformation optics using graphene." Science **332**, 1291–1294 (2011).
15. Q. Bao and K. P. Loh, "Graphene photonics, plasmonics, and broadband optoelectronic devices." ACS Nano **6**, 3677–3694 (2012).
16. T. Otsuji, S. A. Boubanga Tombet, A. Satou, H. Fukidome, M. Suemitsu, E. Sano, V. Popov, M. Ryzhii, and V. Ryzhii, "Graphene-based devices in terahertz science and technology," J. Phys. D **45**, 303001 (2012).

#183562 - $15.00 USD Received 16 Jan 2013; revised 11 Mar 2013; accepted 26 Mar 2013; published 5 Apr 2013

17. B. Sensale-Rodriguez, T. Fang, R. Yan, M. M. Kelly, D. Jena, L. Liu, and H. (Grace) Xing, "Unique prospects for graphene-based terahertz modulators," Appl. Phys. Lett. **99**, 113104 (2011).
18. B. Sensale-Rodriguez, R. Yan, and M. Kelly, "Broadband graphene terahertz modulators enabled by intraband transitions," Nature Comm. **3**, 780–787 (2012).
19. S. H. Lee, M. Choi, T.-T. Kim, S. Lee, M. Liu, X. Yin, H. K. Choi, S. S. Lee, C.-G. Choi, S.-Y. Choi, X. Zhang, and B. Min, "Switching terahertz waves with gate-controlled active graphene metamaterials." Nature Mat. **11**, 936–941 (2012).
20. A. Andryieuski, A. Lavrinenko, and D. Chigrin, "Graphene hyperlens for terahertz radiation," Phys. Rev. B **86**, 121108(R) (2012).
21. R. Alaee, M. Farhat, C. Rockstuhl, and F. Lederer, "A perfect absorber made of a graphene micro-ribbon metamaterial," Opt. Express **20**, 28017–28024 (2012).
22. A. Fallahi and J. Perruisseau-Carrier, "Design of tunable biperiodic graphene metasurfaces," Phys. Rev. B **86**, 195408 (2012).
23. H. Yan, X. Li, B. Chandra, G. Tulevski, Y. Wu, M. Freitag, W. Zhu, P. Avouris, and F. Xia, "Tunable infrared plasmonic devices using graphene/insulator stacks." Nature Nanotech. **7**, 330–334 (2012).
24. B. Sensale-Rodriguez, R. Yan, S. Rafique, M. Zhu, W. Li, X. Liang, D. Gundlach, V. Protasenko, M. M. Kelly, D. Jena, L. Liu, and H. G. Xing, "Extraordinary control of terahertz beam reflectance in graphene electro-absorption modulators," Nano Lett. **12**, 4518–4522 (2012).
25. A. Nikitin, F. Guinea, F. Garcia-Vidal, and L. Martin-Moreno, "Surface plasmon enhanced absorption and suppressed transmission in periodic arrays of graphene ribbons," Phys. Rev. B **85**, 081405 (2012).
26. A. Y. Nikitin, F. Guinea, and L. Martin-Moreno, "Resonant plasmonic effects in periodic graphene antidot arrays," Appl. Phys. Lett. **101**, 151119 (2012).
27. S. Thongrattanasiri, F. Koppens, and F. García de Abajo, "Complete optical absorption in periodically patterned graphene," Phys. Rev. Lett. **108**, 047401 (2012).
28. N. J. Cronin, *Microwave and Optical Waveguides* (Taylor & Francis, 1995).
29. S. Tretyakov, *Analytical Modeling in Applied Electromagnetics* (Artech House Publishers, 2003).
30. J. D. Buron, D. H. Petersen, P. Bø ggild, D. G. Cooke, M. Hilke, J. Sun, E. Whiteway, P. F. Nielsen, O. Hansen, A. Yurgens, and P. U. Jepsen, "Graphene conductance uniformity mapping." Nano Lett. **12**, 5074-5081 (2012).
31. K. F. Mak, L. Ju, F. Wang, and T. F. Heinz, "Optical spectroscopy of graphene: from the far infrared to the ultraviolet," Solid State Comm. **152**, 1341–1349 (2012).
32. L. Ren, Q. Zhang, J. Yao, Z. Sun, R. Kaneko, Z. Yan, S. Nanot, Z. Jin, I. Kawayama, M. Tonouchi, J. M. Tour, and J. Kono, "Terahertz and infrared spectroscopy of gated large-area graphene," Nano Lett. **12**, 3711-3715 (2012).
33. G. Hanson, "Dyadic Green's functions for an anisotropic, non-local model of biased graphene," IEEE Trans. Antennas and Propagation, **56**, 747–757 (2008).
34. I. Llatser, C. Kremers, A. Cabellos-Aparicio, J. M. Jornet, E. Alarcón, and D. N. Chigrin, "Graphene-based nano-patch antenna for terahertz radiation," Photon. Nanostr. Fundam. Appl. **10**, 353–358 (2012).
35. P. Tassin, T. Koschny, and C. M. Soukoulis, "Effective material parameter retrieval for thin sheets: theory and application to graphene, thin silver films, and single-layer metamaterials," Physica B: Condensed Matter **407**, 4062–4065 (2012).
36. CST Computer Simulation Technology AG, http://cst.com .
37. P. D. Cunningham, N. N. Valdes, F. a. Vallejo, L. M. Hayden, B. Polishak, X.-H. Zhou, J. Luo, A. K.-Y. Jen, J. C. Williams, and R. J. Twieg, "Broadband terahertz characterization of the refractive index and absorption of some important polymeric and organic electro-optic materials," Journal of Applied Physics **109**, 043505 (2011).

1. Introduction

Terahertz (THz) radiation provides many useful applications for spectroscopy, biomedical imaging, security, food quality control and communication [1–3]. Since the very field of the THz science and technology is relatively young, new devices and materials are on demand. Graphene, a material consisting of one monolayer of carbon atoms, provides unique properties, such as optical transparency, flexibility, high electron mobility and conductivity, which can be tuned by electrochemical potential via, for example, electrostatic gating, magnetic field or optical excitation [4–6]. It was theoretically shown that graphene supports surface plasmon polaritons in the terahertz and infrared ranges [7–15] and can be a building material for metamaterials, which provide a wider range of electromagnetic properties than continuous graphene. Therefore continuous and structured graphene allows for an ultimate terahertz radiation control resulting in functional devices [16], such as modulators [17–19], hyperlenses [20], tunable reflectors, filters, absorbers and polarizers [21–24]. In this paper we will focus on graphene

#183562 - $15.00 USD Received 16 Jan 2013; revised 11 Mar 2013; accepted 26 Mar 2013; published 5 Apr 2013

absorber.

Even though graphene is optically transparent, it has an enormous absorption of 2.3% per monolayer in the optical range and more in the THz. Absorption of structured graphene films can reach 100% [21–23, 25–27]. In most cases modeling of graphene metamaterial based devices is based on numerical simulation and optimization and requires multiple variables analysis. It not only makes the design process slower and more complicated, but also hinders important physics.

In this paper we propose a simple, yet powerful method for graphene metamaterials description and tunable perfect absorber design. The method is based on the transmission line analogy and describes a graphene metamaterial through an effective surface conductivity. In section II we describe the methodology of the perfect absorber design. We explain the effective surface conductivity approach and examine the properties of graphene wire medium and graphene fishnet metamaterial in section III. Examples of tunable narrow- and broadband absorbers designs are given in section IV.

2. Metamaterials based perfect absorber

The effective surface conductivity approach is based on the transmission line analogy. It is well-known, that propagation of a plane wave in a dielectric can be described by an equivalent transmission line with perfect electric and perfect magnetic boundary conditions [28, 29]. A thin conducting layer with surface conductivity $\sigma_S = \sigma'_S + i\sigma"_S$ at the flat boundary between two dielectrics (refractive indices $n_1$and n_2, see Fig. 1) is equivalent to a load attached to the junction between two transmission lines.

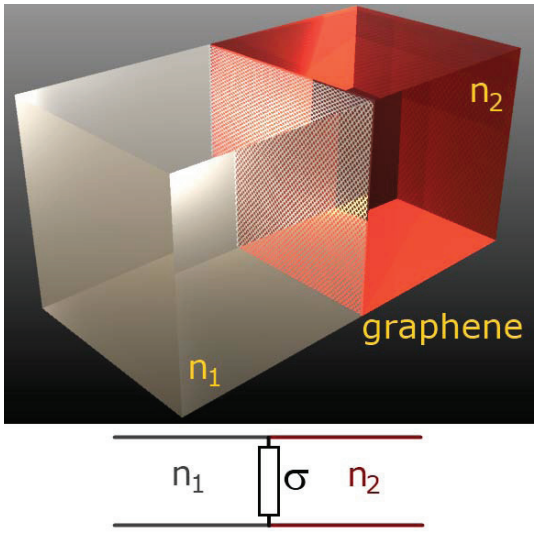

Fig. 1. The conductive interface (for example, graphene layer) between two dielectrics is equivalent to a load attached to the junction between two transmission lines.

If the thickness of the conductive layer is much smaller than the wavelength (that is true for graphene in the ultrabroad range of spectrum from radiowaves to deep ultraviolet), than we can neglect the thickness and consider the conductive layer as a point load. For the normal incidence the amplitude transmission and reflection coefficients for a wave coming from the first dielectric are [18]

#183562 - $15.00 USD Received 16 Jan 2013; revised 11 Mar 2013; accepted 26 Mar 2013; published 5 Apr 2013

$$t = \frac{2n_1}{n_1 + n_2 + \sigma_S Z_0}, \tag{1}$$

$$r = \frac{n_1 - n_2 - \sigma_S Z_0}{n_1 + n_2 + \sigma_S Z_0}, \tag{2}$$

$Z_0 = 120\pi$ Ohm is the free-space impedance. In the case of infinite surface conductivity $\sigma_S = \infty$ the wave will be fully reflected ($r = -1$). Surface conductivity equal to 0 plays no effect and the formulas become standard Fresnel formulas for the interface between two dielectrics. For the incidence at angle ϕ one should consider TE and TM polarizations, then the transmission and reflection coefficients become

$$t_{TE} = \frac{2q_1}{q_1 + q_2 + Z_0\sigma_S}, \tag{3}$$

$$r_{TE} = \frac{q_1 - q_2 - Z_0\sigma_S}{q_1 + q_2 + Z_0\sigma_S}, \tag{4}$$

$$t_{TM} = \frac{2\frac{\varepsilon_1}{q_1}}{\frac{\varepsilon_1}{q_1} + \frac{\varepsilon_2}{q_2} + Z_0\sigma_S}, \tag{5}$$

$$r_{TM} = \frac{\frac{\varepsilon_1}{q_1} - \frac{\varepsilon_2}{q_2} - Z_0\sigma_S}{\frac{\varepsilon_1}{q_1} + \frac{\varepsilon_2}{q_2} + Z_0\sigma_S}, \tag{6}$$

where $q_{1,2} = \sqrt{\varepsilon_{1,2} - \sin^2\phi}$ is the normalized normal component of the propagation constant and $\varepsilon_{1,2} = n_{1,2}^2$ are the relative dielectric constants.

The most important for the practical THz applications is the case of the normal incidence, therefore we focus on it. Let us normalize the formulas for the normal incidence (1) dividing nominator and denominator by the refractive index of the first material n_1

$$t = \frac{2}{1 + \gamma + \xi + i\zeta}, \tag{7}$$

$$r = \frac{1 - \gamma - \xi - i\zeta}{1 + \gamma + \xi + i\zeta}, \tag{8}$$

where $\gamma = n_2/n_1$ is the ratio of the refractive indices and $\xi + i\zeta = (\sigma'_S + i\sigma"_S)Z_0/n_1$ is the normalized surface conductivity.

Structuring graphene layer allows for changing the surface conductivity by reducing the amount of conductive material and by introducing plasmonic resonances. The power transmittance, reflectance and absorbance of the considered conducting layer are

$$T = \gamma|t|^2 = \frac{4\gamma}{(1 + \gamma + \xi)^2 + \zeta^2}, \tag{9}$$

$$R = \frac{(1 - \gamma - \xi)^2 + \zeta^2}{(1 + \gamma + \xi)^2 + \zeta^2}, \tag{10}$$

$$A = 1 - T - R = \frac{4\xi}{(1 + \gamma + \xi)^2 + \zeta^2}. \tag{11}$$

The extremum analysis reveals that maximal absorption occurs, when $\zeta = 0$ and $\xi = 1 + \gamma$, then the absorbance is equal to

#183562 - $15.00 USD Received 16 Jan 2013; revised 11 Mar 2013; accepted 26 Mar 2013; published 5 Apr 2013

$$A_{\max} = \frac{1}{1+\gamma}. \tag{12}$$

For the symmetric environment ($n_1 = n_2$, so $\gamma = 1$) the maximal absorbance cannot exceed 0.5. We can, however, obtain larger absorbance for $\gamma < 1$ that corresponds to the case of incidence from a high-dielectric material with $n_1 > n_2$. For example, $\gamma = 0.29$ for a silicon ($n = 3.416$) - air interface and $A_{\max} = 0.77$. We should, however, take into account that in reality incidence from silicon requires the wave to be previously coupled into silicon from air that gives transmittance 0.70. Therefore, the total absorption of the initial wave is 0.54, that is not much better than for a symmetrical case $\gamma = 1$.

We can achieve larger absorbance if we use more conductive layers separated with a dielectric. In the simplest configuration it can be a graphene metamaterial layer above a mirror (ground plane) [see Figs. 2(a)–2(b)].

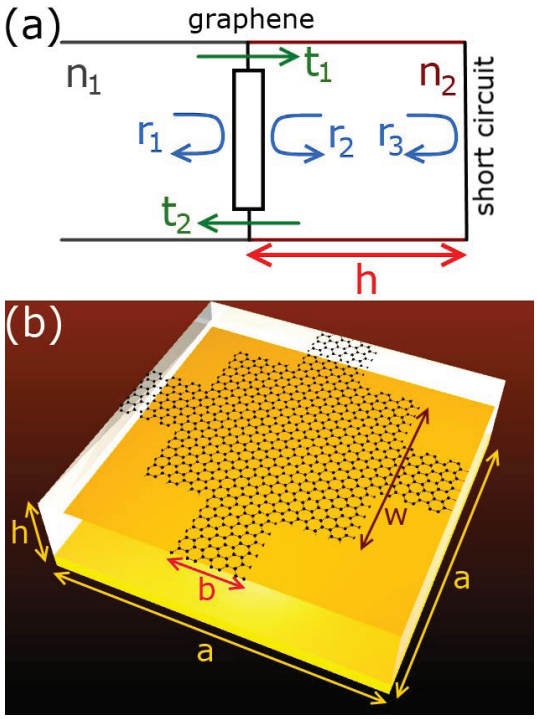

Fig. 2. Total absorbance can be achieved in the graphene metamaterial film above a ground plane. (a) Equivalent transmission line. Graphene metamaterial is equivalent to a load, metallic mirror is equivalent to short circuit. (b) Graphene metamaterial and mirror (ground plane) are separated with a thick dielectric layer of thickness h. The metamaterial itself consists of two layers of structured graphene separated with a very thin dielectric.

In this configuration we have a Fabry-Perot resonator with one perfect mirror ($r_3 = -1$). The reflection coefficient for the whole system is

$$r = r_1 - \frac{t_1 t_2}{\exp(-i2\Phi) + r_2}, \tag{13}$$

where $\Phi = k_0 n_2 h$ is the phase advance upon one propagation through dielectric, $k_0 = \frac{\omega}{c}$ is the free-space wavenumber and h is the thickness of dielectric between graphene and ground

#183562 - $15.00 USD Received 16 Jan 2013; revised 11 Mar 2013; accepted 26 Mar 2013; published 5 Apr 2013

plane. The meaning of the transmission and reflection coefficients t_1, t_2, r_1, r_2 is clear from the Fig. 2(a) and their values are

$$t_1 = \frac{2}{1+\gamma+\xi+i\zeta}, \tag{14}$$

$$t_2 = \frac{2\gamma}{1+\gamma+\xi+i\zeta}, \tag{15}$$

$$r_1 = \frac{1-\gamma-\xi-i\zeta}{1+\gamma+\xi+i\zeta}, \tag{16}$$

$$r_2 = \frac{\gamma-1-\xi-i\zeta}{1+\gamma+\xi+i\zeta}. \tag{17}$$

After simple though tedious algebraic transformations we obtain absorbance

$$A = \frac{4\xi}{(1+\xi)^2+[\zeta+\gamma\cot(\Phi)]^2}. \tag{18}$$

The absorbance can be equal to 1 if simultaneously

$$\xi = 1, \tag{19}$$

$$\zeta+\gamma\cot(\Phi) = 0. \tag{20}$$

Absorbance as a function of ξ and $\zeta+\gamma\cot(\Phi)$ has one global maximum (Fig. 3). We define the working regime of the absorber, when absorbance $A \geq 0.9$. The working range of ξ and $\zeta+\gamma\cot(\Phi)$ lies within a circle of the radius ≈ 0.7 centered at $\xi = 1.2$, $\zeta+\gamma\cot(\Phi) = 0$. We should keep in mind that $\xi(\omega, E_F)$ and $\zeta(\omega, E_F)$ are the functions of frequency ω and Fermi energy E_F, whereas $\cot(\Phi) = \cot(\frac{\omega}{c} n_2 h)$ is just the function of frequency only.

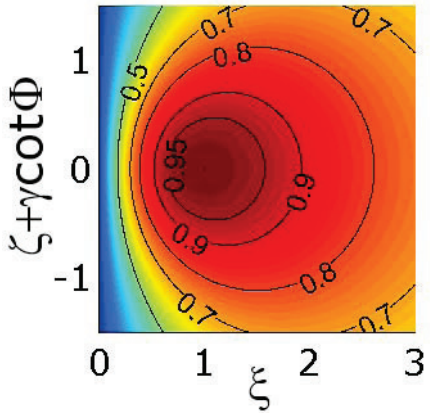

Fig. 3. Absorbance shows a global maximum at $\xi = 1$, $\zeta+\gamma\cot(\Phi) = 0$. The working range $A \geq 0.9$ lies within a circle of the radius ≈ 0.7 centered at $\xi = 1, \zeta+\gamma\cot\Phi = 0$.

For the further discussion we should look in more details at the properties of graphene and graphene metamaterials.

3. Effective conductivity of graphene metamaterials

It is very natural to describe the properties of graphene in terms of surface conductivity, since this quantity can be measured directly in a wide range from radio to THz frequencies [30–32]. Graphene's conductivity is described with interband and intraband contributions [33, 34]

#183562 - $15.00 USD Received 16 Jan 2013; revised 11 Mar 2013; accepted 26 Mar 2013; published 5 Apr 2013

$$\sigma_S = \sigma_S^{intra} + \sigma_S^{inter}, \tag{21}$$

$$\sigma_S^{intra} = \frac{2k_BTe^2}{\pi\hbar^2}\ln(2\cosh\frac{E_F}{2k_BT})\frac{i}{\omega + i\tau^{-1}}, \tag{22}$$

$$\sigma_S^{inter} = \frac{e^2}{4\hbar}[H(\frac{\omega}{2}) + i\frac{4\omega}{\pi}\int_0^\infty \frac{H(\Omega) - H(\frac{\omega}{2})}{\omega^2 - 4\Omega^2}d\Omega], \tag{23}$$

where $H(\Omega) = \sinh(\frac{\hbar\Omega}{k_BT})/[\cosh(\frac{\hbar\Omega}{k_BT}) + \cosh(\frac{E_F}{k_BT})]$, T is the temperature, E_F - electrochemical potential (Fermi energy), ω- frequency of the electromagnetic wave and $\tau = 10^{-13}$ s - the relaxation time. For the THz frequencies, where the photon energy $\hbar\omega \ll E_F$, the interband part (23) is negligible comparing to the intraband. Therefore, in the THz range graphene is well described by the Drude-like surface conductivity (22). For $E_F \gg k_BT$ the conductivity depends linearly on the Fermi energy

$$\sigma_S \approx \frac{e^2E_F}{\pi\hbar^2}\frac{i}{\omega + i\tau^{-1}}. \tag{24}$$

For the numerical simulations graphene is usually represented as a layer of material of a small thickness Δ with an in-plane effective permittivity

$$\varepsilon_{eff,t} = 1 + i\frac{\sigma_S}{\varepsilon_0\omega\Delta}. \tag{25}$$

The normal component of the effective permittivity $\varepsilon_{eff,n} = 1$.

In other words we can say that graphene is represented by a thin metal with the plasma frequency depending on the Fermi level

$$\omega_P = [\frac{2e^2k_BT}{\pi\hbar^2\varepsilon_0\Delta}\ln(2\cosh\frac{E_F}{2k_BT})]^{1/2}. \tag{26}$$

The conductivity of a continuous graphene film can be calculated analytically with expression (22). However, for structured graphene metamaterials an analytical description is problematic and therefore we should turn to numerical methods. Tassin et al. [35] proposed to characterize the thin-film metallic and graphene metamaterials with the electric and magnetic effective surface conductivities $\sigma_\parallel^{(e)}$and $\sigma_\parallel^{(m)}$ and proposed the formulas for their retrieval for the symmetric environment (the same homogeneous dielectric on the both sides from the metasurface). In this work we consider the normal incidence of the wave and a thin-film electric metamaterial in the asymmetric environment. In this situation the formula for the restoration of the effective surface conductivity σ_S^{eff}, which can be derived through the inversion of the Eq. (7), becomes

$$\xi + i\zeta = \frac{2}{t} - (1 + \gamma). \tag{27}$$

Some numerical programs (like, for example, CST Microwave Studio [36], which we used) calculate S_{21}-parameter that is related to the amplitude transmission coefficient, as $S_{21} = \sqrt{\gamma}t$. The effective surface conductivity expressed through S_{21}-parameter is

$$\sigma_S^{eff}Z_0 = \frac{2}{S_{21}}\sqrt{n_1n_2} - (n_1 + n_2). \tag{28}$$

We should mention that while the refractive index of the ambient dielectrics is of little importance for the restoration of continuous graphene surface conductivity (we do not consider

#183562 - $15.00 USD Received 16 Jan 2013; revised 11 Mar 2013; accepted 26 Mar 2013; published 5 Apr 2013

the influence of the substrate on the electronic structure and Fermi level), it becomes crucial for the graphene metamaterial, since the frequency of the plasmonic resonance depends on the dielectric surrounding. Therefore, n_1 and n_2 should correspond to dielectrics that are involved in the device fabrication.

Let us now look on values of the surface conductivities of graphene and graphene based metamaterials (Fig. 4). We should, however, make a comment on choosing the design of metamaterials. First of all, in order to tune their properties by electrostatic gating, there should be at least two layers of graphene separated with a thin dielectric spacer. Each of the graphene sheets then plays the role of a gate electrode. Applying the voltage moves the Fermi level in both graphene layers [18], but in opposite directions. Nevertheless, if initially the Fermi level is at the Dirac point, the changes of graphene conductivity in both layers are the same. Employing the ground plane [Fig. 2(b)] as a gate electrode does not suit, since as we will see further the dielectric separation between graphene metamaterial and ground plane should be on the order of several tens of micrometers, that requires high gating voltages of tens of kV for noticeable change in conductivity.

Second, structured graphene layer should be electrically connected, otherwise we cannot change the properties of the whole layer by applying voltage. Therefore metamaterials, consisting of isolated graphene patches are not suitable for tunable devices.

Third, in order to make the metamaterial polarization insensitive (under normal incidence), its unit cell should be at least C_4 symmetric.

This is why we consider two-dimensional graphene wire medium [wires width $b = 2\mu$m, see Figs. 4(b) and 2(b)] and graphene fishnet [wires width $b = 2\mu$m, patches width $w = 12\mu$m, see Figs. 4(c) and 2(b)]. The sizes are selected to be compatible with photolithography. Nevertheless, much finer structures can be fabricated with electron-beam or nanoimprint lithography. The period of the metamaterial is $a = 15\mu$m. Graphene is embedded into TOPAS polymer ($n_1 = n_2 = 1.53$), which has low losses in the THz range [37]. Graphene is modeled as a layer of thickness $\Delta = 2$ nm.

The conductivity of continuous graphene is Drude-like and it changes gradually with the frequency and Fermi level [see Fig. 4(a)]. Naturally, graphene wires [Fig. 4(b)] exhibit lower values of conductivity, as graphene is effectively "dissolved" in dielectric. The fishnet metamaterial [Fig. 4(c)] exhibits a strong plasmonic resonance. The resonance frequency increases with the Fermi energy that corresponds to the fact that graphene becomes "more metallic". In the resonant region the real part of conductivity becomes large and the imaginary part experiences oscillations and even changes its sign becoming negative. We should mention that the wire medium [Fig. 4(b)] also exhibits a plasmonic resonance, but it occurs at higher frequencies. Moreover, we observe here the fundamental plasmonic mode. Higher order modes lie at larger frequencies and they can also be used for the THz absorber [21].

4. Graphene metamaterial based absorber

Now we focus on the design of a graphene metamaterial based absorber. Practically the Fermi level can be changed by electrostatic gating by approximately ± 0.5 eV, so we consider $E_F = 0.5$ eV as the Fermi energy value where we expect the maximal absorption, while for Fermi level at the Dirac point $E_F = 0$ eV we expect the minimal absorption. We consider the graphene double layer metamaterial above the ground plane depicted in Fig. 2(b).

For some applications an absorber should be narrowband, for others the bandwidth should be broad. Therefore we will formulate the guidelines for the bandwidth tuning by design. We have already mentioned that the absorbance has a global maximum near $\xi = 1$, $\zeta + \gamma \cot\Phi = 0$. The working bandwidth depends on how fast ξ and $\zeta + \gamma \cot\Phi$ change with frequency ω. For the gradually changing conductivity of continuous graphene film [see Fig. 4(a)] the fastest

#183562 - $15.00 USD Received 16 Jan 2013; revised 11 Mar 2013; accepted 26 Mar 2013; published 5 Apr 2013

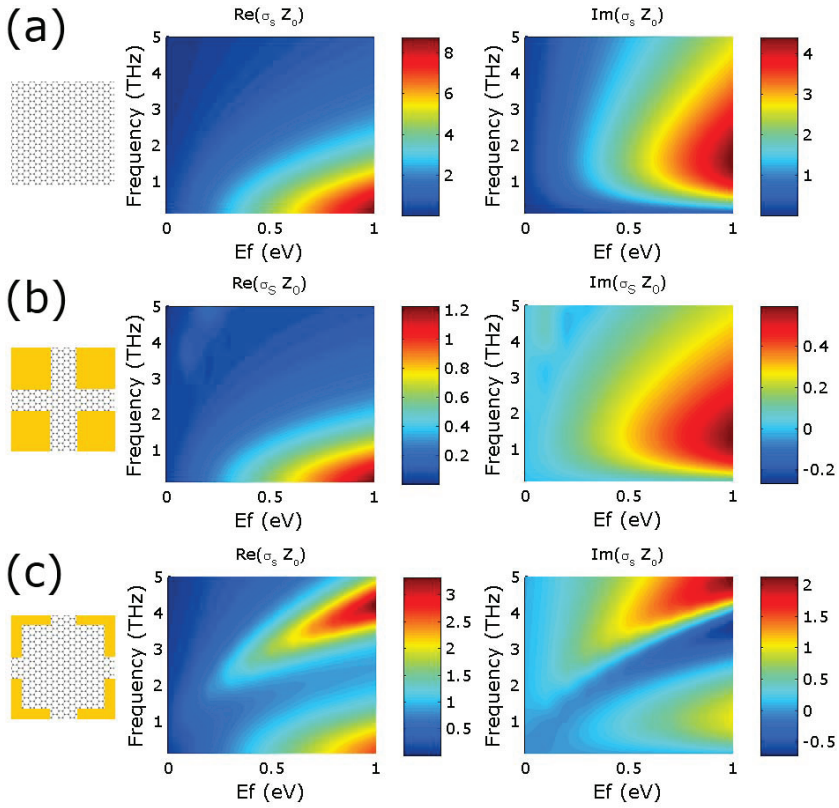

Fig. 4. Real and imaginary part of normalized effective surface conductivity $\sigma_S Z_0$ of continuous graphene (a), graphene wire medium (b) and graphene fishnet metamaterial (c). In all cases there are two layers of graphene separated with a thin dielectric. Graphene wire medium shows reduced Drude-like conductivity as compared with continuous graphene, whereas graphene fishnet exhibits a plasmonic resonance that gives large values of real part and negative imaginary part of conductivity.

changes are related to $\cot\Phi = \cot(\frac{\omega}{c} n_2 h)$, so the cotangent, which is monotonously decreasing function, determines the working bandwidth mostly. To extend the bandwidth we can, however, compensate the quick variation of cotangent $\cot(\frac{\omega}{c} n_2 h)$ by modifying the frequency behavior of $\zeta(\omega)$ that depend on design (see Fig. 4).

The design procedure of the absorber is the following. First, from the extracted effective conductivity dependence $\xi(\omega)|_{E_F=0.5eV}$ we find the working frequency ω_0 corresponding to $\xi(\omega_0)|_{E_F=0.5eV} = 1$. Second, we select the thickness h of the dielectric such, that $\zeta(\omega_0)|_{E_F=0.5eV} + \gamma\cot(\frac{\omega_0}{c} n_2 h) = 0$. That gives $h = \frac{c}{n_2\omega_0}\mathrm{arccot}(-\frac{\zeta(\omega_0)|_{E_F=0.5eV}}{\gamma})$. If $\mathrm{arccot}(-\frac{\zeta(\omega_0)|_{E_F=0.5eV}}{\gamma}) < 0$, then we should add π, since the thickness cannot be negative. Finally we check the performance of the absorber with the Fermi level E_F variation.

If we look at the continuous graphene film, its conductivity components ξ and ζ change gradually [Figs. 5(a)–5(b)]. The required dielectric thickness is $h = 35.9\mu$m. The sum of a gradually changing ζ [Fig. 5(b), green line] with quickly changing $\gamma\cot\Phi$(orange line with triangles) is also a quickly changing function (red line with circles). Therefore the working bandwidth of the absorber [Fig. 5(c), orange line with triangles] is narrow, namely, 0.4 THz.

#183562 - $15.00 USD Received 16 Jan 2013; revised 11 Mar 2013; accepted 26 Mar 2013; published 5 Apr 2013

The results of the analytical predictions [Fig. 5(c), lines] are in a perfect agreement with the full-wave numerical modeling [Fig. 5(c), symbols]. We should admit that at frequencies close to 1.2 THz there is a pronounced absorption of 0.4 even in the off-state, when Fermi energy is 0. It occurs due to the high values of real conductivity. Nevertheless, at the working point 2.3 THz absorbance changes from less than 0.1 to 1 in the range of Fermi energy variation from 0 to 0.5 eV. What is important, the frequency of high absorbance lies very close to the minimum of absorbance, which is defined by the optical length $n_2 h$ through the $\cot\Phi = \infty$ condition. Therefore, the absorbance is very sensitive to the value of $n_2 h$ in this region and it allows to use the absorber as an efficient sensor, which reacts to the changes of refractive index n_2 or thickness h.

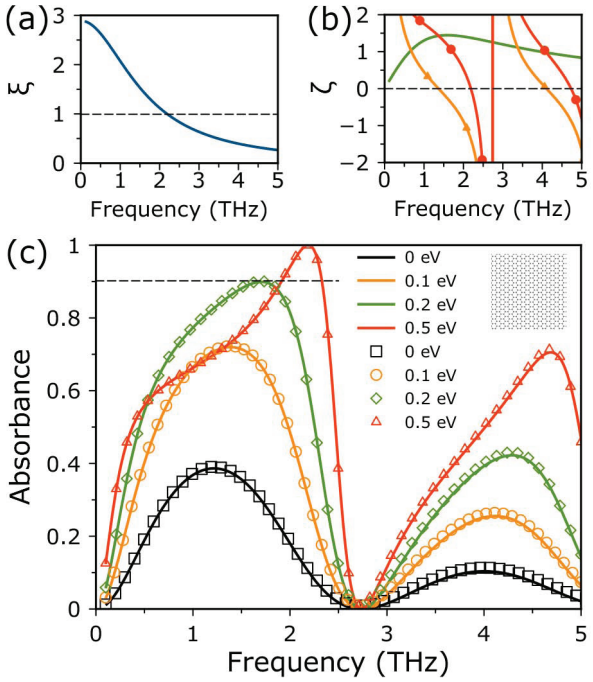

Fig. 5. (a) Real part of normalized surface conductivity of two graphene layers $\xi = 1$ at 2.3 THz. (b) Imaginary part ζ (green line) defines the value of dielectric thickness h, so that quickly changing $\gamma\cot\Phi$(orange line with triangles) compensate ζ and give $\zeta + \gamma\cot\Phi = 0$ (red line with circles) at the same frequency 2.3 THz. (c) Absorbance of the device is tuned by Fermi energy [0 (black), 0.1 (orange), 0.2 (green), 0.5 (red) eV]. The analytical predictions (lines) are in a perfect correspondence with full-wave simulation results (symbols). The working bandwidth at $A \geq 0.9$ is 0.4 THz.

Employment of graphene wire medium leads to a similar absorber performance as for the continuous graphene film, since their conductivities dependence on frequency and Fermi energy are qualitatively the same [see Figs. 4(b)–4(c)]. We can, however, tune the working frequency (condition $\xi(\omega) = 1$) by changing the width of graphene wires b. Another situation occurs for the graphene fishnet, which has the plasmonic resonance (Fig. 6). Even though in the low-frequencies the real conductivity ξ is below 1 [Fig. 6(a)], in the region of plasmonic resonance $\xi \approx 1$. The imaginary part ζ [Fig.6(b), green line] oscillates and has a region of quick increase with the frequency. For the working thickness of dielectric $h = 17.6\mu$m it is therefore possible to compensate monotonously decreasing $\gamma\cot\Phi$ [Fig.6(b), orange line with triangles] and the sum

#183562 - $15.00 USD Received 16 Jan 2013; revised 11 Mar 2013; accepted 26 Mar 2013; published 5 Apr 2013

$\zeta + \gamma\cot\Phi$ [Fig.6(b), red line with circles] stays close to 0 in a wider range than for continuous graphene. Therefore the working bandwidth at $A \geq 0.9$ reaches 1.9 THz [Fig. 6(c)]. Tuning the Fermi energy allows for gradual variation of the absorbance from 0.05-0.2 to 1. Such device can be used as a tunable broadband THz attenuator.

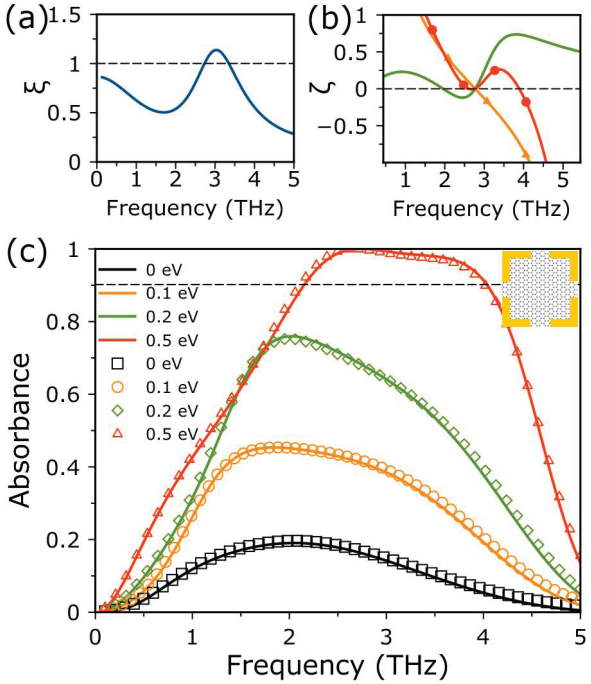

Fig. 6. (a) Real part of normalized surface conductivity of two graphene fishnet layers $\xi = 1$ at 2.7 THz. (b) Imaginary part ζ (green line) defines the value of dielectric thickness h, so that quickly changing $\gamma\cot\Phi$(red line with circles) compensate ζ and give $\zeta + \gamma\cot\Phi = 0$ (orange line with triangles) at the same frequency 2.7 THz. (c) Absorbance of the device is tuned by Fermi energy [0 (black), 0.1 (orange), 0.2 (green), 0.5 (red) eV]. The analytical predictions (lines) are in a perfect correspondence with full-wave simulation results (symbols). The working bandwidth at $A \geq 0.9$ is 1.9 THz.

5. Discussion and conclusions

We have presented the description of graphene metamaterials through the effective surface conductivity. Such description is rather natural, since the surface conductivity can be directly measured in experiment. Using the effective conductivity for reflection and transmission allows for simple and efficient design of graphene based functional THz devices. Even though we have focused on the THz range due to its technical importance and need for new THz materials and devices, the presented approach is valid for other frequencies, such as radio-, microwaves, infrared and visible ranges.

In this work we considered only normal incidence of electromagnetic waves, but the approach can be easily extended to an oblique incidence with the TE and TM reflection and transmission coefficients (6). It is important, however, that the diffraction effects are negligible.

As an example, we demonstrated the THz absorbers based on continuous graphene and graphene fishnet. In the former case the continuous graphene layer above a ground plane works as a narrowband absorber (bandwidth 0.4 THz), while the employment of the plasmonic res-

#183562 - $15.00 USD Received 16 Jan 2013; revised 11 Mar 2013; accepted 26 Mar 2013; published 5 Apr 2013

onance in a structured graphene metamaterial allows for a broadband tunable absorber (bandwidth 1.9 THz).

A wide range of other terahertz devices can be described with the effective surface conductivity approach: modulators, tunable filters, polarizers, polarization converters, sensors, etc. We believe, that this approach will become a useful tool for the emerging field of graphene terahertz photonics.

Acknowledgments

The authors thank D. Chigrin, J.C. Due Buron, F. Pizzocchero and S. Zhukovsky for useful discussions. A.A. acknowledges the financial support from the Danish Council for Technical and Production Sciences through the GraTer (11-116991) project.

#183562 - $15.00 USD Received 16 Jan 2013; revised 11 Mar 2013; accepted 26 Mar 2013; published 5 Apr 2013